AN INVESTIGATION OF SLAG FLOATATION AND ENTRAPMENT IN A CONTINUOUS CASTING TUNDISH USING FLUID FLOW SIMULATIONS, SAMPLING AND PHYSICAL METALLURGY

Henrik Solhed[1, 2)], Lage Jonsson[1, 3)]

[1)] MEFOS, Box 812, SE-971 25 Luleå, Sweden
[2)] Dept. of Physics, Luleå University of Technology, Sweden
[3)] Dept. of Materials Science and Eng., KTH, Stockholm, Sweden

Key words: Steel, slag, clean-steel, tundish, fluid-flow, mixing, theory, models, sampling, microscope-studies

ABSTRACT

Some aspects of inclusion behavior in the tundish have been investigated both theoretically and experimentally. Good agreement was obtained between measured and predicted temperature and flow fields for one- to six-strand continuous casting tundishes. In this study the flow field was redesigned with weirs, resulting in the addition of a vertical component to the Stoke's equation. The results indicate an increase in the velocity at which inclusions rise (smaller inclusions (< 20 μm)). Consideration of slag, flux and refractory in the model it has also made it possible to simulate the mixing of steel and slag. Special sampling techniques were used to gather information. Samples were analyzed using ultrasonic testing, LOM, SEM and Atomic Force Microscopy (AFM). The analysis results were used to verify the predictions regarding steel/slag mixing and understanding of physical conditions at the interfaces. As a result, the casting praxis was improved (cleaner steel) and the products were of higher quality.

1 INTRODUCTION

Extensive efforts have been made in academia and industry over the last decades to exploit and enhance continuous-casting tundish systems with respect to their metallurgical performance. As a consequence, numerous physical and mathematical modelling studies embodying both industrial and water-model tundishes have been done and reported in the literature. Recently, Mazumdar and Guthrie made a review [1] covering these modelling efforts of continuous-casting systems. They pointed out that a modern day steel-making tundish should be designed to provide maximum opportunity for carrying out various metallurgical operations such as inclusion separation, flotation, alloy trimming, inclusion modification, superheat control, as well as thermal and particulate homogenisation. Furthermore, they concluded that mathematical studies indicate that flow conditions conducive to the removal of non-metallic inclusions from tundishes can be created inserting appropriate flow-modification devices. The optimal design and location of flow modifiers with respect to clean steel is clearly dependent on tundish geometry [2] as well as the operating conditions and is very dependent on the steel inclusions' size range.

In the models reported on, the refractory has however rarely been included and, to the knowledge of the authors, neither the flux nor liquid slag has so far been included in any modelling efforts. It is obvious though, that both the refractory and the slag layer preferably should be an integrated part of the model for appropriate understanding of many metallurgical issues like thermal and inclusion behaviour as the slag and the refractory are both potential sources, sinks and modifiers for inclusions. Furthermore, a useful approach to modelling fluid flow in the slag phase enables studies of heat and fluid-flow conditions coupled with thermodynamics in the very important steel/slag region (from a metallurgical point of view) in a continuous casting tundish. The alternative to coupling fluid flow and thermodynamics would be to use the two-film theory [3-7]. However, use of the surface-renewal theory to couple thermodynamics and fluid flow might not be adequate when slag and metal are mixed, and certainly wouldn't allow for study of the mixing itself. Therefore, as a first step towards a process model of a continuous-casting tundish, a model of a tundish built on the basis of fundamental equations which takes slag, flux and refractory into account has been developed and is presented in this paper.

Specifically, the model reflects the penetration of the steel and slag phases into each other and other conditions at the slag/metal interface. Many authors have studied the dispersion of the slag phase into the steel using physical modelling [8-15]. Among them Kim, Fruehan and Guthrie [13] determined a critical stirring rate for the break up of the interface in a ladle. From their results it is evident that the interface is fully disintegrated and a mixing zone establishes above a certain stirring rate, but it can also be deduced that a certain degree of mixing exists even for low flow rates. Furthermore, Spalding and Villasenor [16] have shown, using a long duct of rectangular cross-section and two fluids of different densities, that the instability that arises due to the presence of shear between the fluid layers will cause a mixing of the layers. They also showed that this instability could be predicted by a fluid-flow calculation, if the position of the interface was calculated. The present authors used these ideas to incorporate the liquid slag phase into their model of a continuous-casting tundish. The predictions of heat and fluid flow were validated by comparison with both velocity and temperature measurement data from production-scale tundishes. Furthermore, the fluid-flow model including the slag phase has been validated by investigation of steel-slag samples taken with a special sampling device[17]. Studying these samples also revealed some information on steel-inclusion interaction.

The mathematical modelling is described in section 2. Thereafter, in section 3 the solution procedure including initial and boundary conditions are discussed. The flow and temperature field results are presented in section 4. In section 5 the slag entrapment results are described as well as the sampling technique, the methods used to investigate the samples and the results of the investigation. Finally, section 6 includes a discussion of the presented results, section 7 some conclusions and section 8 some suggestions on future work.

2 MATHEMATICAL MODELLING

The continuous-casting tundish has increasingly evolved into a very useful reactor for steel refining. However, the operating conditions, high temperature and visual opacity of liquid steel make it hard to make direct experimental investigations. Mathematical modelling is a reasonable alternative to investigate fluid-flow and heat transfer phenomena in continuous-casting tundishes. Today, a large number of modelling efforts covering various aspects like fluid flow, residence time, inclusion and thermal energy transport, etc have been reported in the literature. These works have led to considerable improvements in our understanding of the various transport processes associated with tundish operations. However, most of the modelling efforts have not included the refractory, slag, or flux. Considering refractory, slag and flux in the model should for one hand render a better prediction of heat and fluid flow, but most importantly make it possible to couple thermodynamic calculations on inclusion chemistry, solidification processes etc. with macro-kinetics derived from first principles. This has been the driving force for the development of the model of a continuous-casting tundish, which besides the steel phase also takes the refractory, slag and flux into account. The basic ideas behind the development of the model are given in section 2.1 and the conservation equations in section 2.2. The property variations of the different phases are given in section 2.3 together with the other auxiliary equations and in section 2.4 the boundary conditions are stated.

2.1 Basic ideas behind the modelling

Below is a summary of some of the thinking behind the development of the model.

To sustain process variations and obtain desirable chemistry conditions it is necessary to have the right and homogenous temperature at the inlet, near the slag and at the outlet. The regions of homogeneity should be as large as possible. The temperature field is strongly influenced by the velocity field. Near the outlet, the velocity field has to be as vertical and symmetric as possible to prevent clogging. Near the steel/slag interface the transport should be almost horizontal and calm. This can be attained using flow guides to redesign the flow field.

The consideration of refractory, slag and flux makes it possible to do conjugate heat-transfer calculations right out to the surfaces. Heat conducted to the outermost surface can be heat-exchanged to the surroundings. This is modelled by using temperature-dependent radiative and convective boundary conditions resulting in a physically more correct solution. Solidification at cold parts of the innermost surfaces can be considered in the models. Refractory surfaces suffering from erosion and/or dissolution might be taken into account. Including the refractory in the calculation would also be advantageous in that it would make it possible to use IR techniques for some validation purposes.

The mixing of slag and metal in a zone where the velocities are low is thought to originate from the instability that arises when two streams of fluid, with stable density differences, flow

past one another. The presence of shear leads to instability, which is characterised by the growth of waves, later rolling up into (small) vortices. This shear instability, "The Kelvin-Helmholtz Instability", may serve as the mechanism of mixing between the layers, promoting the vertical transport of properties such as heat or reactants. Furthermore, Spalding and Villasenor [16] have showed, using a long duct of a rectangular cross-section and two fluids of different densities, that this instability could be predicted with a fluid-flow calculation if the position of the interface was calculated. Using these ideas as the basis for the modelling approach, a mathematical model of continuous casting tundish could be extended to include the slag phase. This development enables predictions of fluid-flow and heat-transfer conditions in the highly important steel/slag region.

2.2 Conservation equations

The Model is steady or unsteady and is based on conservation equations for:

Conservation of mass

$$\frac{\partial r}{\partial t} + \nabla \cdot (r \cdot \vec{V}) = 0 \tag{1}$$

where ρ is density and $\vec{V}$ is velocity

Conservation of momentum

$$r \cdot \frac{D\vec{V}}{Dt} = -\nabla p + \vec{B} + m \cdot \nabla^2 \vec{V} \tag{2}$$

where p is pressure, B is volume force and μ is dynamic viscosity

Conservation of energy

$$r \cdot \frac{De}{Dt} - \vec{\nabla} \cdot k\vec{\nabla}\vec{T} - \vec{\nabla} \cdot \left(\sum_j r D_j \cdot e_j \cdot \vec{\nabla} m_j \right) - m \cdot \Phi - \frac{DP}{Dt} - S = 0 \tag{3}$$

where e is the static enthalpy, k is the thermal conductivity, T the absolute temperature, μ is the dynamic viscosity, S is the source function (i.e. the thermal energy created per unit volume) and

$\Phi = \left(\frac{\partial u_i}{\partial x_j} + \frac{\partial u_j}{\partial x_i} - \frac{2}{3} \frac{\partial u_l}{\partial x_l} d_{ij} \right) \frac{\partial u_i}{\partial x_j}$ is the dissipation function. The first and last term in the dissipation function within the brackets come from the viscous part of the normal stresses, whereas the second term comes from the shear stresses.

Conservation of elements in each phase

$$r \cdot \vec{V} \cdot \frac{D n_a}{Dt} = \vec{\nabla} \cdot \left(\sum_j r D_j \cdot n_{a,j} \cdot \vec{\nabla} m_j \right) \tag{4}$$

where n_α is the mass fraction of element α in mixture of compounds, D_j is the mass diffusion coefficient for component j. $n_{\alpha,j}$ is the mass fraction of element α in a compound substance j and m_j is the mass fraction (concentration) of substance j in mixture.

Turbulent transport equations

The LVEL algebraic turbulence model is a unique feature (built into PHOENICS) useful for conjugate-heat-transfer problems. Far away from the wall, it reduces to the well-established result [18]:

$$v^+ = K \cdot y^+ \tag{5}$$

where v^+ is the dimensionless effective viscosity and K is the von Karman constant (0.417) and y^+ is the dimensionless distance from the wall.

2.3 Auxiliary equations

Property variations of the steel phase

density
The temperature dependent density of steel is described by the following expression [19]:

$$\rho_l = 8.586\text{x}10^3 - 0.8567T_l \tag{6}$$

where T_l is the temperature of the steel.

heat capacity
The temperature dependent heat capacity is calculated as [20]:

$$C_{p,Fe} = (452.963 + 176.704\text{x}10^{-3}T_l - \frac{482.082\text{x}10^5}{T_l^2}) \tag{7}$$

dynamic viscosity
The temperature dependent dynamic viscosity is calculated as [19]:

$$\mu_{l,l} = 0.3147\text{x}10^{-3}\exp\left(\frac{46480}{8.3144T_l}\right) \tag{8}$$

where T_l is the temperature of the steel.

Property variations of the liquid slag phase

The following typical slag composition was chosen for the calculations: 50 % CaO, 12.5 % Al_2O_3, 7.5 % MgO and 30 % SiO_2.
heat capacity
The temperature dependent heat capacity for slag is calculated as [21]:

$$C_{p,CaO} = \frac{4.1868\text{x}10^3}{56.079}(11.86 + 1.08\text{x}10^{-3}T_s - \frac{1.66\text{x}10^5}{T_s^2}) \tag{9}$$

$$C_{p,Al_2O_3} = \frac{4.1868x10^3}{101.961}(28.804 + 2.197x10^{-3}T_s - \frac{11.56x10^5}{T_s^2}) \quad (10)$$

$$C_{p,SiO_2} = \frac{4.1868x10^3}{60.084}(17.119 + 0.452x10^{-3}T_s - \frac{9.335x10^5}{T_s^2}) \quad (11)$$

$$C_{p,MgO} = \frac{4.1868x10^3}{40.304}(11.707 + 0.751x10^{-3}T_s - \frac{2.734x10^5}{T_s^2}) \quad (12)$$

$$Cp_s = (\%CaO)C_{p,CaO} + (\%Al_2O_3)C_{p,Al_2O_3} + (\%MgO)C_{p,MgO} + (\%SiO_2)C_{p,SiO_2} \quad (13)$$

where T_s is the temperature of the slag.

dynamic viscosity

The temperature dependence of the dynamic viscosity for the slag is given by the following expression [22]:

$$\mu_{l,s} = 1.0 \cdot \exp\left(-5.589 + \frac{24323.7}{T_s} - 0.7099 \cdot \ln(T_s)\right) \quad (14)$$

where T_s is slag temperature.

Treatment of the liquid slag phase

General equations

Incorporation of the slag phase into the model of the tundish has been done using the following two equations [23, 24, 25 26]:

$$\frac{\partial}{\partial t}(r_l c_1) + div(r_l \vec{V}_l c_1) = 0 \quad (15)$$

$$\frac{\partial}{\partial t}(r_s c_3) + div(r_s \vec{V}_s c_3) = 0 \quad (16)$$

where $\vec{V}_l$ is the velocity vector for the steel phase and $\vec{V}_s$ is the velocity vector for the slag phase. The variable c_1 has, at time zero, the value 1 in the regions where there is steel only and has the value 0 in the regions where there initially is only slag. Similarly, c_3 has the values 0 and 1 in the regions where the tundish initially contains only steel and slag, respectively. The volume of steel per unit mass, V_{st}, and the volume of slag per unit mass, V_{sl}, are calculated as follows [23]:

$$V_{st} = \frac{c_1}{c_1 + c_3}\frac{1}{\rho_{st}} \quad (17)$$

$$V_{sl} = \frac{c_3}{c_1 + c_3} \frac{1}{\rho_{sl}} \tag{18}$$

where ρ_{sl} is the density of the slag and ρ_{st} is the density of steel. The total volume of the liquid phase (steel and slag) per unit mass is given by [23]:

$$V_{tot} = V_{st} + V_{sl} \tag{19}$$

Treatment of the solid slag phase (flux)

The computational area where covering powder blocks the flow is set to have the following physical properties [27]:

density	600 kg/m^3
specific heat	1180 J/kg°K
thermal conductivity	1.7 W/m°K
thermal expansion	0

2.4 Boundary Conditions

The boundary conditions for a solution are given below. The most decisive are:

The fixed mass flow at the inlet

The mass flux at the inlet is the product of the velocity (m/s) and the density (kg/m^3) usually set in the first cell-layer.

The constant pressure at the outlet

At the outlet, the desired pressure normally is the dynamic pressure. Therefore it is convenient to set the reference pressure to zero.

The frictional flow near the lining

At the fluid/solid interfaces fully developed friction is set.

The emissivities and heat transfer coefficients for slag- and tundish surfaces

The heat transfer takes part both through the lining and through the flux. The lining is usually 4-layered and results in the following expression:

$$\theta_s - \theta_g = \frac{1}{k} \cdot \frac{\phi}{A} \qquad \frac{1}{k} = \frac{1}{\alpha_s} + \sum_1^n \frac{\delta_i}{\lambda_i} + \frac{1}{\alpha_g} \tag{20}$$

where θ_x is temperature at different layers (s is steel, g is surrounding gas), k is heat transmission coefficient, α_s and α_g are heat transfer coefficients at steel-refractory and outer surfaces respectively (W/m^2°C), δ_i is thickness of layer i (m), λ_i is thermal conductivity for material i (W/m°C), ϕ is heat flow rate (W) and A is the area of conducting cross section (m^2).

The heat energy entering the outer surfaces is heat exchanged to the surrounding through three mechanisms:

$$\varphi = \varphi_{gs} + \varphi_{sw} + \varphi_c \qquad (W/m^2) \qquad (21)$$

where φ_{gs} is radiation exchange with radiating gas-volume (can be neglected), φ_{sw} is radiation exchange with tundish walls, ladle bottom and surrounding walls and φ_c is natural convection with the gas near the tundish walls.

In case the ladle bottom or other parts of reactors are warmer than the flux surface, then a positive heat exchange to the tundish will take place.

Radiation exchange
The radiation exchange is given by the formula below [28)]:

$$\varphi_{sw} = \sigma \cdot \varepsilon_{sw} \cdot \left(\theta_s^4 - \theta_w^4\right) \qquad (22)$$

where

$$\varepsilon_{sw} = \varepsilon_s \cdot \varepsilon_w \cdot \tau_{gm} \cdot \beta_{sw} + \Delta\varepsilon_{sw} \qquad (23)$$

and where σ is Stefan-Boltzman's constant (W/m^2K^4), ε_s is the emissivities for flux and tundish walls, ε_w is the emmissivities for influencing walls, τ_{gm} is $1-A_{gm}$ (can be set to 1 in air and in the absence of flames), A_{gm} is the mean absorption number for surrounding gas due to radiation from the surfaces, β_{sw} is the view factor (=1 at plane and not shadowed surfaces), $\Delta\varepsilon_{sw}$ is flame radiation contribution (can be neglected), θ_w is the wall temperature and θ_s is surface temperature.

Convective exchange
The convective exchange regards the heat exchange to the gas near the surfaces of the tundish, the shroud, the SEN and also the flux surface. The exchange is taken to occur as natural or slightly forced convection. The mathematical expression is:

$$\varphi_c = \alpha_s \cdot (\theta_g + \Delta\theta_g - \theta_s) \qquad (24)$$

where α_s is convective heat transfer coefficient ($W/m^{2\circ}C$) and $\Delta\theta_g$ is θ_g(measure point) minus θ_g(near surface).

The emmissivities are measured with thermovision-camera to around 0.85 for the flux and to ca 0.93 for the outer surfaces of the tundish. The convective heat transfer coefficient is empirically set to 10-15. The surface losses are than in the range 10-25 kW/m^2.

Simple measurements with spot-meter or contact-pyrometer ought to be enough for verification. For more exact validation a measurement with thermovision-camera is preferred.

3 SOLUTION

The commercial, sequential or parallel program [29], PHOENICS is used to solve the mathematical equations. A well-posed problem is usually solved within 10-30 hours with one CPU. The elapsed time can be reduced to 4-12 hours with three CPU's.

3.1 Numerical Method

The grids are developed as Multi-Block-Fine Grid Embedded (MB-FGE) grids [18]. The main grid can be divided in parts and specific objects can have a finer grid. Though the staggered-grid method is the most common, the Collocated Covariant Method (CCM)- and Generalised Collocated Velocity (GCV)- methods are also used, the former especially in conjunction with the Length-Velocity (LVEL) model. The effective viscosity calculation in the LVEL-model [18] is based on the distance from the nearest wall, the local velocity and the laminar viscosity. In the GCV-method, structured grids are linked in an unstructured way. This method is used in cases where grid-influenced convergence is undesirable.

3.2 Initial conditions

Initially, the species content for each cell is defined in an input-file, as well as the physical and/or metallurgical properties. Solved for variables are given expected values in the entire calculation domain.

3.3 Convergence criteria

The number of sweeps guided the convergence. The number of sweeps was adjusted to be large enough to give the last change of all values less than 10^{-4}-10^{-5} times the value itself. Usually 1500-2500 sweeps were necessary to fulfil the criteria.

4 FLOW- AND TEMPERATURE FIELD RESULTS

Almost all of the properties of steel, slag and refractory are temperature dependent. Therefore a good prediction of temperature is necessary for reliable predictions of other quantities. The flow field in a tundish strongly influences the temperature field. Earlier studies were aimed at verifying predictions [2] of both the fluid-flow and the temperature fields. However, the flow-field verifications were rather expensive. Infrared temperature measurements on the outer surfaces and the observation of hot spots have instead often been relied upon for verification purposes. The hot spots indicate that the fluid flow is hitting the surface more or less perpendicularly at those positions, thus giving an indication of the flow field (Fig. 4.1).

4.1 Prediction

Fig. 4.2 shows how the flow field modified by weirs results in an improved temperature distribution. A baffle prevents the re-circulating of colder steel on its way towards the inlet. The result is a uniform high temperature at the inlet and instead of a 10-20 degree temperature gradient at the outlet, a homogeneous and symmetric temperature distribution in 3 dimensions is achieved. The temperature at the steel/slag interface is also improved with respect to chemical reactions.

At the end of each heat the velocity field at the inlet (Fig. 4.2) enhances the removal of slag particles dispersed in the steel. The removal of slag is furthermore facilitated by the use of the turbulence killer and the small dam. This results in a modified momentum in the vertical direction, which in addition to the rising of the slag velocity according to the Stoke's equation promotes slag flotation. Also, the calm passage at the steel/slag interface makes it probable that only a small amount of slag penetrates into the steel flow (cf. chap. 5). Finally, at the outlet it can be seen that the velocities are fairly vertical and symmetrical around the outlet opening. This is believed to hinder small inclusions from clogging the seat of the SEN and the SEN itself.

Fig. 4.3 shows temperature contours for a 2-strand tundish in a simulation done after refractory, slag and flux were implemented in the model. Currently both refractory and slag powder are included. Thus, it has become possible to consider solidification at those parts of the tundish wall having a wall temperature below the liquidus temperature.

4.2 Verification

All predicted results are considered unreliable until a models is verified, which is when all predicted entities are verified. Different verification techniques have to be used for different predicted entities.

The thin-film carbon-rod technique [30)] was used to verify the velocity field. Finding a good measurement position was a difficult task but with guidance by means of the prediction it was possible to find a homogeneous non-turbulent position. Another difficulty was obtaining a correct calibration of the rods for the low-velocity conditions in near laminar measurement positions. Fig. 4.4 shows measured and predicted velocities as a function of depth between the slag and the bottom of a tundish in such a position. The thin-film theory is not adequate for velocities under 1 cm/s (which is the limit of the calibration). That's why the agreement is not so good just below the slag and just above the bottom. The best agreement between predictions and measurements would be achieved if the rods were included in the simulation model and a one-sided comparison made.

Thermocouples of almost equal calibration were selected for the temperature-field measurements, both in the fluid and in the refractory. The temperature is shown in Fig. 4.5 at three depths, approximately 10 cm inside the fluid. Since the refractory and slag powder have been included in the model it has been much easier to verify both temperature and velocity models. As mentioned above, this can now be done by direct measurement of emissivities, surface temperatures and observation of hot spots.

Near-stationary temperature profiles in different refractory layers could also be measured by installing a number of thermocouples inside the lining. In Fig. 4.6 the measured temperatures are compared with the corresponding predictions.

When both velocities and temperatures are verified the question arises of whether the calculations could be used to enhance the design of the tundish in such a way that the steel quality is improved. Fig. 4.7(a)-4.7(b) show how the production praxis is influenced. Fig. 4.7(c) indicates that the steel cleanness, based on total oxygen analyses, is improved by 10 ppm. The difficulty was to get the samplers to take samples in the same way, i.e. the reproducibility. To be fully convinced more appropriate experiments have to be done.

Fig. 4.8-4.9 probably show an endothermic slag being built upon an exothermic nucleus. Apparently, larger slag particles are floating up whilst small ones follow the steel flow.

5 SLAG FLOTATION AND ENTRAPMENT RESULTS

The slag/steel-mixing zone is a mixture between the tundish slag and exothermic ladle slag, floated exothermic and/or endothermic inclusions as well as the tundish steel including rising inclusions. The fluid flow is physically governed by the equations in section 2. The variables solved are the concentration variables representing slag and steel. The predicted values should be comparable with a momentary flow-field situation. Also, it should be possible to identify the mixing mechanisms at the interface from the samples taken.

5.1 Prediction

First a preliminary solution was obtained with a reasonable converged velocity field without solving for the concentration variables governing the flow in the slag/steel mixing zone. Thereafter, the full solution was obtained by restarting from the preliminary solution.

Fig. 5.1 shows the predicted slag concentration in steel below the slag layer. The situation next to the ladle shroud penetrating into the tundish is interesting. It can be seen that the concentration profile follows the flow field, indicating that slag is pulled down by the down-flow. The figure also indicated that slag fringes may transport slag to the incoming downwardly directed high-velocity flow. This transport probably results in some entrapment of slag droplets.

Fig. 5.2 shows the slag concentration in the uppermost steel layer (3 mm down in steel). The figure further indicates that slag, though low in concentration, penetrates into the steel as a result of the velocity field. Near the walls the upwardly flowing steel instead pushes steel towards the slag. Along the symmetry plane, near the stopper rods and near the ladle shroud, there are downwardly directed velocity components facilitating the downward transport of slag.

A reasonable question is how it is possible at all for penetration of slag into steel to occur at these low, almost horizontal, velocities (cf. Chap 5.2.4)?

5.2 Measurements

The slag model, being a fairly new model component, puts new demands on the verification technique and analyses. The interpretation of the concentration distribution revealed suitable positions for sampling. However, sampling at the steel/slag and steel/refractory interfaces is not easy. Inexpensive sampling techniques have so far not been reported. Therefore, a simple re-useable sampler MISS (Momentary Interfacial Solidification Sampling) was developed and used for low-carbon steel grades. Based on old and new ideas, efforts have also been made to develop a suitable analysis technique.

5.2.1 Sampler and sampling

The sampler is described in an internal MEFOS report [17]. Mainly it consists of a 120-mm long square (8x80 mm) pipe with a mass that ensures adequate cooling. Since the sample

should not be heated, the sampler must be properly insulated. Moreover, to avoid turbulence at the surface of the sample, the interior must be etched for good wetting conditions.

When the sampler is immersed into the liquid at the correct speed, the result is a flat or slightly convex slag surface. For low-carbon steel 0.5 seconds is suitable. After 3-5 seconds the sampler is lifted and cooled after which the sample is released.

5.2.2 Sample Preparation and Ultrasonic Study

The samples are heat treated to obtain good structural homogeneity. Surfaces are machined plane parallel. The entrance surface should be machined very well.

Ultrasonic immersion testing techniques are used to analyse the samples. The instrument used for this study is a Branson Krautkramer USIP20HR with a high frequency option. The probe frequency is 50MHz with a 0.5" focal length (in water). Two flat-bottom holes (FBH) of 70 and 50 μm were used for calibration. This instrument consists of a high-frequency point-focused probe, an immersion tank with an X-Y scanning-probe and a PC-based data collection and evaluation system. The inspected zone depth is 1.3 mm in the centre of the sample. The inspection zone is determined by physical properties of the probe and ends in both directions when half of the energy is lost, which happens when the energy drop is -6dB (decibel). The resulting C-scan (the PC image) is then used for evaluation. The evaluation is based upon experience from earlier testing. A-scan and time of flight (instrument screen) is used as a complement to the C-scan during evaluation. In A-scan porosity often produces multiple peaks while inclusions usually produce a single peak.

The ultrasonic testing is used to get a coarse overview of rising inclusions, penetration of slag particles into steel and unwanted pores. The entrapped slag particles may also be earlier floated exothermic, endothermic or mixed slags. Fig. 5.3 shows typical ultrasonic testing results compared with corresponding predicted results. The sample is taken approximately 50 mm from the surface of the ladle shroud and penetrating 120 mm down into the steel. Apparent similarities are found with regards to the predicted flow and concentration fields (cf. Fig. 5.1). The upper surface is the steel/slag interface and has a remaining thin slag layer attached to the steel, probably being the mixing zone.

5.2.3 Light-microscope Studies

For examination by LOM mainly a Micro-Vickers was used. The purpose was to get an overview of the MISS plates at magnification of 150x as well as details of different areas at magnification 600x. That equipment is also used for hardness tests. The most important use was the marking of interesting details as inclusions. This was also necessary for location of the object to be examined by AFM. SEM analyses for identification usually preceded this location marking.

5.2.4 SEM Studies

These studies are mainly used for analysis of the involved components in regions or within specific inclusions. This is a prerequisite for further examination with the AFM technique.

Fig. 4.8 shows a rising slag particle indicated by the wake. Probably the inclusion is unstable because smaller alumina particles break off during its path to the top slag. Fig. 4.9 is a detail of the same inclusion showing how Ca-Al and oxides are built on a nucleus of Cr-Ti.

Fig. 5.4 is a picture of the steel/slag interface showing significant instability of the slag/metal interface. Fig. 5.5 is a detail of such an instability. The region was determined to contain salts (Na- and K-salts) and oxides (mainly Fe-, Al-, Si-oxides).

The thin slag layer (mixing zone) was determine to have a lot of Al next to the steel body but also much Fe in higher slag layers as is shown in Fig. 5.6. This probably indicates the existence of a mixing zone adjacent to the steel body.

Finally, Fig. 5.7 illustrates X-ray mappings of the three positions marked in Fig. 5.3. The maps indicate that there is an increasing content of Al and Si from the first position to the third.

5.2.5 AFM Studies

The principal of AFM is the same as for most profilometer techniques, a sharp tip scanning the surface collects height data. The primary exception is the highly sensitive positioning mechanism moving the tip or the sample, and the extremely small tips sensing the surface. The most common position technique is the use of a piezo tube for the movement in all directions, x-y and z. An x-y-motion goes up to about 125 μm. A z-direction motion goes up to around 5-8 μm. The tips are usually of pyramidal shape made with the same techniques as integrated circuits. They have a typical radius in the range of 10-50 nm. To be able to scan with such a small tip without breaking it the force is measured from the bending of a cantilever holding the tip. By sensing the deflection of light from a laser and a four-segmented photodiode (normally), the force can be kept constant. The resolution of the AFM is in the range of a few Ångströms for a crystal-like ordered surface (of course highly dependent on the shape of the tip). For more irregular surfaces a resolution ranging in the order of one to a couple of nanometers is more likely.

The advantage of using AFM is that no special sample preparation is required. The sample can be viewed in vacuum, air, liquid or gas, and it can be non-conductive or conductive. Friction, adhesion, hardness and electric or magnetic properties can be measured besides the topography. The ability to zoom in from macro-scale (125 μm) to nanometer scale makes the AFM a very sensitive tool for the study of inclusions and the formation of micro-cracks in steel. Typical images of inclusions in steel can be seen in Fig. 5.8-5.9.

Fig. 5.8 shows a MnS inclusion in a perlite structure. Bonds, perpendicular to the surrounding matrix can be seen. The clustered structure of the inclusion is obvious. Fig. 5.9 is a picture of clustered Al oxides. The clusters apparently avoid the surrounding matrix, thus creating voids. Bonds are probably found only at positions where the matrix is distorted.

6 DISCUSSION

In Fig. 4.4 and 4.5, the predictions made by the present model show good agreement comparing measured and predicted velocities and temperature in liquid steel. The statement made by Mazumdar and Guthrie that a reasonable mathematical framework now exists for predicting flow and the associated transport processes therefore appears to apply also for the present model of a continuos casting tundish. In this model, the refractory has been incorporated in the calculation domain to achieve the future possibility to model steel-refractory interaction.

As seen in Fig. 4.6, there was also good agreement between measured and predicted refractory temperatures. With reliable model predictions at hand, a comparative analysis of the effect of different configurations of flow guides in a specific tundish can be done with respect to processes like inclusion floatation merely by studying the predicted flow pattern for each configuration. Demonstrated in Fig. 4.2 is such an example of the successful use of model predictions to configure flow-guides that lead to improved fluid-flow and temperature profiles, thus resulting in a reduction of the total oxygen content (≈10 ppm). In summary, in most cases it seems possible to improve inclusion flotation for each specific tundish by choosing a suitable configuration of flow-guides determined from inspection of model predictions.

However, a more precise evaluation of the steel cleanness should render a quantitative comparison of inclusion separation, production, size distribution, composition statistics etc. Therefore, as a first step, the liquid slag phase and flux were added to the present model in addition to the refractory. This resulted in model predictions of small but significant slag concentration in steel close to the steel/slag interface, as shown in Fig. 5.2. The predictions even indicated some slag entrapment close to the ladle shroud, as seen in Fig. 5.1. These results then need to be verified. Therefor, a new sampling technique (MISS) was developed in order to sample the slag/metal interface in a vertical cross section through the interface. With this technique a sample with the shape of a rectangular plate showing a nearly instantaneous picture of the steel/slag interface could be obtained and studied by US, LOM, SEM and AFM techniques.

As noted, apparent similarities were found when comparing the result from the US study shown in Fig. 5.3 with the corresponding prediction of flow- and concentration profiles shown in Fig. 5.1. This could be taken as evidence that the predicted slag concentrations were quite reliable. However, further and more detailed studies of the sample were necessary to confirm the conditions at the slag/metal interface. Fig. 5.4 shows a SEM- picture of the slag/metal interface. The shape of the interface in the figure is very complicated but yet shows a pattern that is pretty much the same as could be expected from the "The Kelvin-Helmholtz Instability" characterised by growth of waves, later rolling up into (small) vortices. This can assume to substantiate that the understanding of the physics upon which the model is based is principally correct. Fig. 5.5 shows a magnified picture of one of the vortices at the interface. In this picture the expected shape of the instability is readily recognised. Also seen in the figure are some particles that appear to be slag droplets torn off from the slag by the instability. Thus, referring to the question posed in section 5.1, it seems possible for slag penetration into steel to occur at these low, almost horizontal, velocities. To even further strengthen our understanding of the situation near the ladle shroud, SEM analyses at different positions as marked in Fig. 5.3 were made. The result of the analyses can be seen in Fig. 5.7. The figure shows that the Al-Si content increases by increasing position number, i.e. from 1 to 3. These results also confirm that the predicted and measured concentrations show the same behaviour.

The complicated shape of the interface might on one hand be due to the irregularities in density, and on the other hand there might be other mechanisms promoting the formation of mixing. For example, Richardson and Brimacombe [31] have shown that turbulence is established in the interfacial region as a direct result of certain reactions and the corresponding transfer, which occurs in addition to turbulence, induced by the fluid flow. This interfacial turbulence arises when the reactions taking place involve surface-active substances. An eddy at the interface may raise or lower the interfacial tension locally, thereby causing contraction or stretching of the micro-scale interface, thus setting up turbulence at the physical bounda-

ries. This leads to phase mixing, which can occur without stirring or macroscopic velocities at the phase boundaries. This micro-scale phenomenon could also distort the expected pattern and it is not considered in the present model of a continuos-casting tundish.

The presented illustration of the conditions at the slag/metal interface has some important implications for understanding both inclusion separation/flotation and slag entrapment in the tundish. Inclusion separation to slag seems not to be a simple process represented by separation against a flat surface, but a complex process where the inclusions are trapped for some time at the interface itself by instability of the slag-metal interface and turbulence fluctuations. Slag particles might be engulfed by steel at the interface as a consequence of instability of the slag-metal interface and these particles could divide into numerous new inclusions, as illustrated in Fig. 4.8. The figure shows an entrapped and rising 30 μm inclusion, with a Cr-Ti core, that splits up into numerous small Ca-Al and Al-O inclusions (a detailed picture of that inclusion can be seen in Fig. 4.9).

7 CONCLUSIONS

A model of a continuous casting tundish, which, besides the steel phase, also considers refractory, slag and flux, has been developed and presented together with the basic ideas behind the development. The model was verified with velocity and temperature measurements in steel and refractory. The agreement between measured velocities and temperatures and the corresponding predictions was good.

In order to verify the fluid flow modelling of the slag phase, a new sampling technique (MISS) was developed. This technique was used to sample the slag-metal interface in a vertical cross section, from the slag-metal interface and downwards to a depth of 10-12 centimetres. MISS samples studied in US, LOM, SEM and AFM verified the fluid flow modelling of the slag phase and the understanding of the physics upon which the model is based.

With verified and reliable model predictions at hand, it has been shown that a comparative analysis of the effect of different configurations of flow guides in a specific tundish can be done with respect to processes like inclusion floatation just by studying the predicted flow pattern for each configuration. Thus, it seems possible to improve inclusion flotation for each specific tundish by choosing a suitable configuration of flow guides determined from inspection of model predictions.

Further, some conclusions can be drawn regarding the conditions close to the slag/metal interface in a continuos casting tundish from the MISS samples and the combined use of US, LOM, SEM and AFM techniques. For example, inclusion separation to slag does not seem to be a simple process represented by separation against a flat surface, but a complex process where the inclusions are trapped for some time at the interface itself by instability of the slag-metal interface and turbulence fluctuations. Moreover, the slag particles might be engulfed by steel at the interface as a consequence of instability of the slag-metal interface and these particles could divide into numerous new inclusions, coalesce or become separated.

8 FUTURE WORK

The next step in future development is to combine the fluid-flow calculation with relevant thermodynamic modelling, for example re-oxidation during the filling process. Also, modelling of growth and separation of inclusions should be incorporated into the model of a continuous casting tundish.

Separate models of ladles, tundishes and moulds do not allow modelling of the connection between process parameters in some reactor and the final product quality. Therefore, a combined model of these reactors should be developed. This would make it possible to study the influence of any specific parameter on the final product.

To trace the influence of a change in a specific process parameter on the product quality, it is necessary to take samples (MISS or LSHR) in the different reactors and to perform detailed analysis (US, LOM, SEM and AFM) of the samples. In this way changes of process parameters could be coupled to product quality. This is an on-going project at MEFOS.

Illustrating the possibilities to study steel-inclusion interaction, two types of inclusions in a MISS sample were inspected by AFM technique, one MnS inclusion (Fig. 5.8) and one alumina inclusion (Fig. 5.9). In the figures it can be seen that the MnS inclusion apparently has many bonds to its surrounding matrix (Fig. 5.8) while the alumina inclusion most probably has bonds only at lattice defects and furthermore seems to cause voids (Fig. 5.9).

9 ACKNOWLEDGEMENT

Thanks to TO23-24, JK2343/97 and FB2340 for financial and technical support and toSSAB Tunnplåt AB, Luleå for the supply of samples and OVAKO Steel, Hofors for the supply and US-analysis of samples. Thanks are also given to the Dept. of Materials and Manufact. Eng. at Luleå University of Technology for supporting the analysis work. The authors would furthermore like to thank Professor Pär Jönsson at Dept. of Materials Sci. and Eng., KTH, Stockholm for fruitful discussions and for initiating the project while working at MEFOS. Finally, Dr Nils Almqvist at Dept. of Physics, Luleå University of Technology is acknowledged for his interest in and support of the AFM-studies.

10 REFERENCES

1) D Mazumdar, R.I.L. Guthrie: The Physical and Mathematical Modelling of Continuous Casting Tundish Systems, *ISIJ International*, **39** (1999), 524.
2) H. Solhed, B. Wahlberg, P. Jönsson: Fifth Int. Conf. on Clean Steel 1997:2:1-10, Balatonszeplak, Hungary.
3) Prandtl L, Über Flüssigkeitsbewegung bei sehr kleiner Reibung, Verhandl. d. III Int. Mathematiker-Kongress Heidelberg 1904, Leipzig 1905, 484-491
4) Higbie R, The rate of absorption of a pure gas into a still liquid during short periods of exposure. Trans. Am. Inst. Chem. Eng. 31 (1935), 365-389
5) Danckwerts P.V, Significance of liquid-film coefficients in gas absorption. Ind. Eng. Chem. 43 (1951) 1460-1467
6) Machlin E S, Kinetics of vacuum induction refining theory. Trans. Metall. Soc. AIME 218 (1960), 314-326

7) Kraus Th., Über den Mechanismus des Stoffaustausches zwischen einem hochverdünnten Gas und dessen Lösung unter besonderer Berücksichtigung der Entgasung von Metallschmeltzen im Vakuum. Schweiz. Arch. Angew. Wiss. Tech. 28 (1962), 452-460
8) Asai S, Kawachi M, Muchi I. Scaninject III, MEFOS, Sweden, (1983), 12:1.
9) Mazumdar D, Nakajiima H, Guthrie R.I.L. Metal. Trans. B, 19 (1988), 507.
10) Sahajwalla V, Brimacombe J.K., Salcudean M.E. Proc. Steelmaking Conf., USA (1989), 497.
11) Mietz J, Schneider S, Oeters F. Steel Res., 62 (1991), 1.
12) Mietz J, Schneider S, Oeters F. Steel Res., 62 (1991), 10.
13) Kim S-H, Fruehan R.J., Guthrie R.I.L., Iron Steelmaker, (1993), 71.
14) Cramb A.W., Jimbo I. Scaninject VII, MEFOS, Sweden, (1995), 89.
15) Xiao Z, Peng Y, Liu C. Chin. J. Mater. Sci. Technical, 3, (1987), 187.
16) Spalding DB, Villasenor F. Numerical Simulation of Kelvin-Helmholtz Instability in a Stratified Shear Flow. PhysicoChemical Hydrodynamics 1987:9:1/2:379-386.
17) B. Wahlberg, H. Solhed: Internal MEFOS-report in Swedish, TM00013K, Mars, 2000.
18) Phoenics ver. 2 "Encyclopaedia", CHAM Ltd, London (1994).
19) Handbook of Physico-chemical Properties at High Temperatures, eds. Y. Kawai and Y. Shiraishi, The Iron and Steel institute of Japan, Japan, (1988), 2.
20) G.Ye: TDCALC, A thermodynamic calculation program for metallurgists and chemists, MEFOS report MF92047, (1992).
21) B.C. Allen, in "Liquid Metals – Chemistry and Physics" (S.Z. Beer, ed.), p. 161, Dekker, New York, 1972.
22) S. Seetharaman, Du Sichen and J.Y. Zhang: JOM, 51, No. 8, (1999), 38-40.
23) L. Jonsson and P. Jönsson, *ISIJ International*,**36** (1996),1127
24) L. Jonsson, C-E Grip, A. Johansson and P. Jönsson: Three-phase (steel, slag, gas) modelling of the CAS-OB process, Proc. 80th Steelmaking Conf., Chicago, USA, April 1997.
25) Hallberg M, Jonsson Lage and Alexis J, "Modeling of hydrogen and sulphur refining during vacuum degassing in a ladle furnace", SCANMET I, Luleå, June 7-8, 1999.
26) Alexis J, Jönsson P G, Jonsson Lage, "A model of an induction-stirred ladle accounting for slag and surface deformation", *ISIJ International*, **39** (1999), 772.
27) Christer Nilsson, SSAB Tunnplåt AB, Luleå, Sweden, Private Communication.
28) Solhed H., Leden B.: Internal MEFOS-report in Swedish, BTF84027B, June 1984.
29) http://www.gmd.de/SCAI, search for Down-Port.
30) R.G. Olsson et. al.: Rate of Dissolution of Carbon in Molten Fe-C Alloys, Trans. Of the Metallurgical Soc. of AIME, vol236, April 1966, pp. 426-429.
31) Richardson F.D., "Drops and Bubbles in Extractive Metallurgy", Metallurgical Transactions, vol. 2, pp. 2747-2756

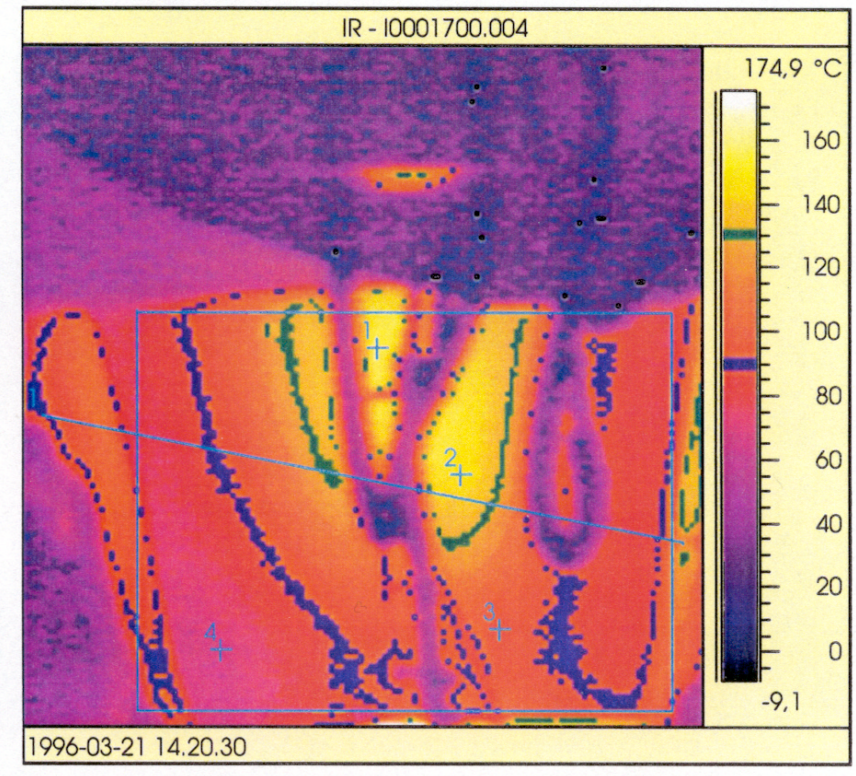

Fig. 4.1(a) - An infrared picture showing surface temperatures and hot spots on the plate surface at the outlet end of a tundish.

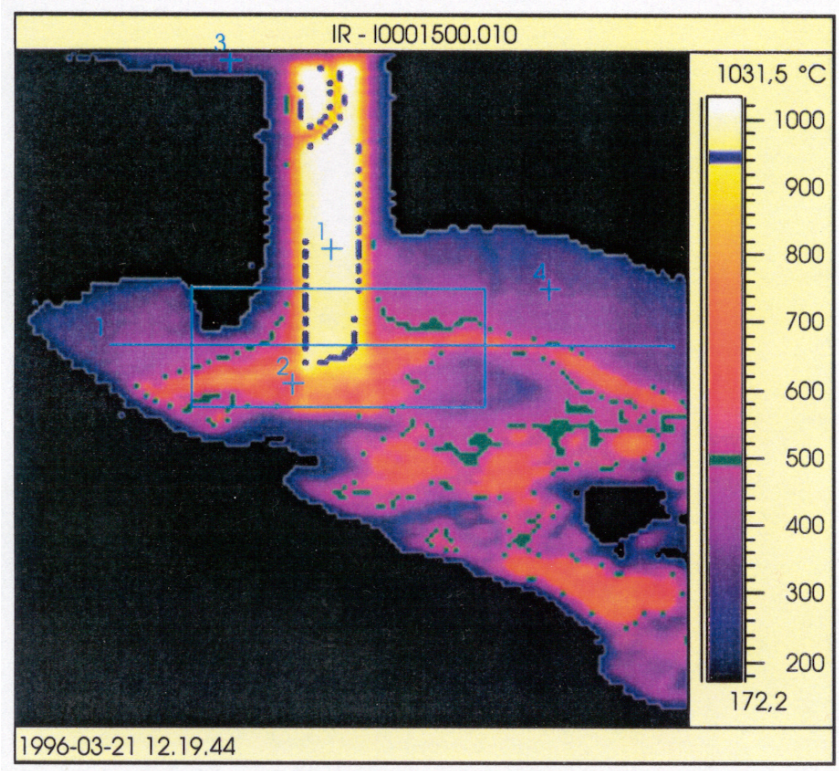

Fig. 4.1(b) - An infrared picture showing temperatures on flux, ladle-shroud and hot spots.

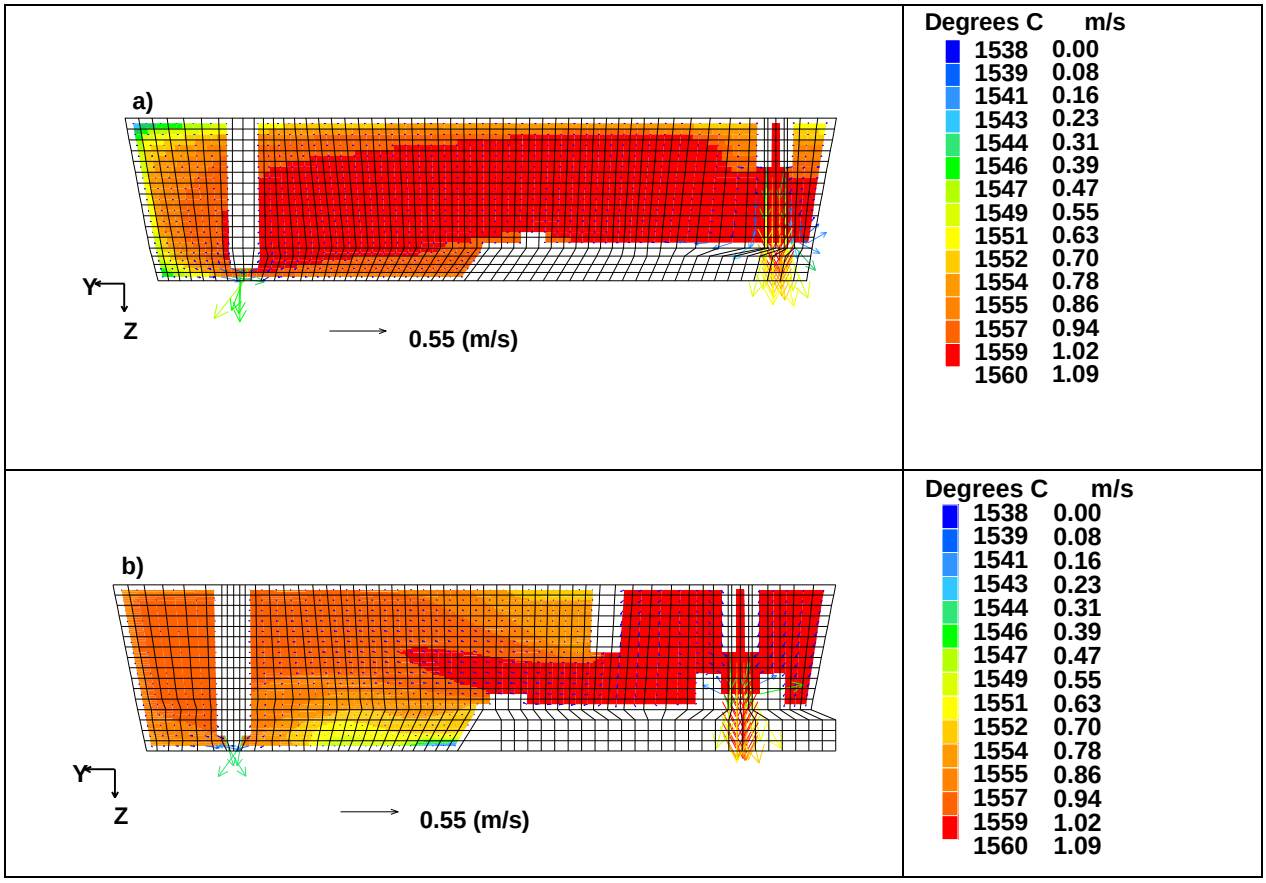

Fig. 4.2 - Velocity vectors superimposed on temperature profiles of a) a normal praxis and b) a modification of the flow field with weirs.

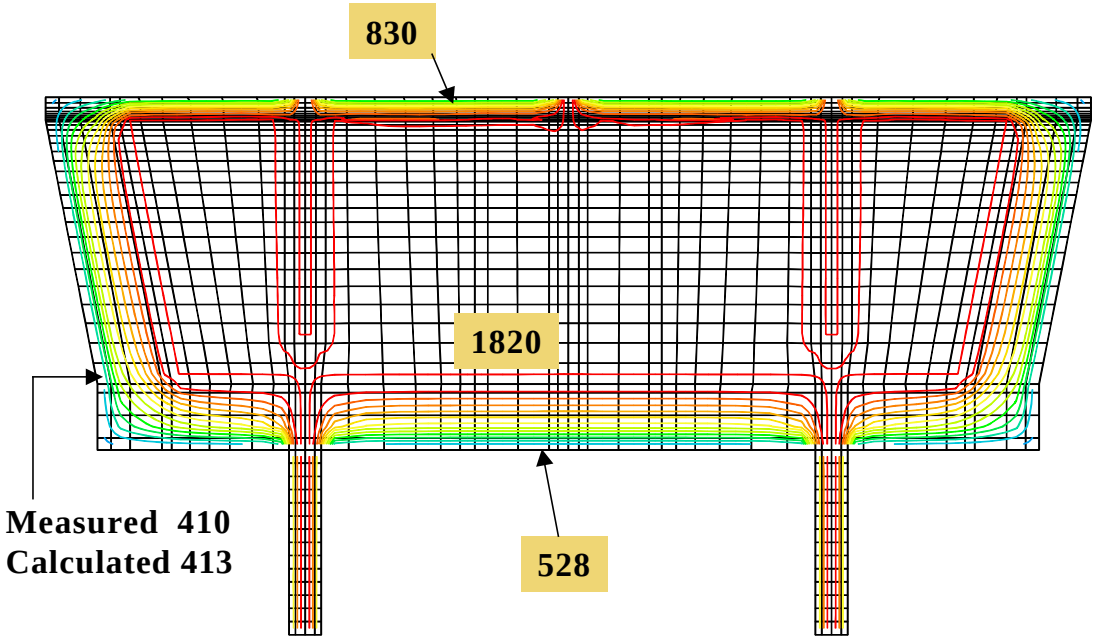

Fig. 4.3 - Isotherms in slag, powder and refractory in a 2-strand tundish and also in the two SENs.

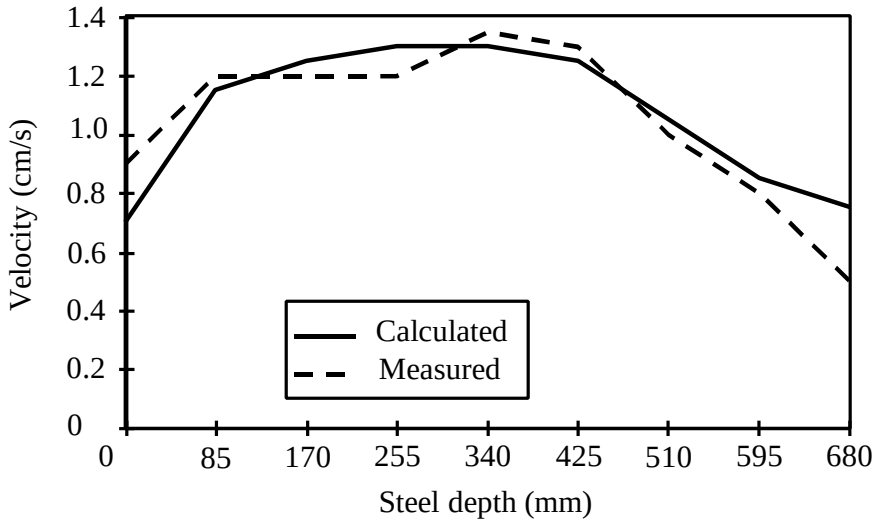

Fig. 4.4 - Predicted and measured steel velocities as a function of steel depth.

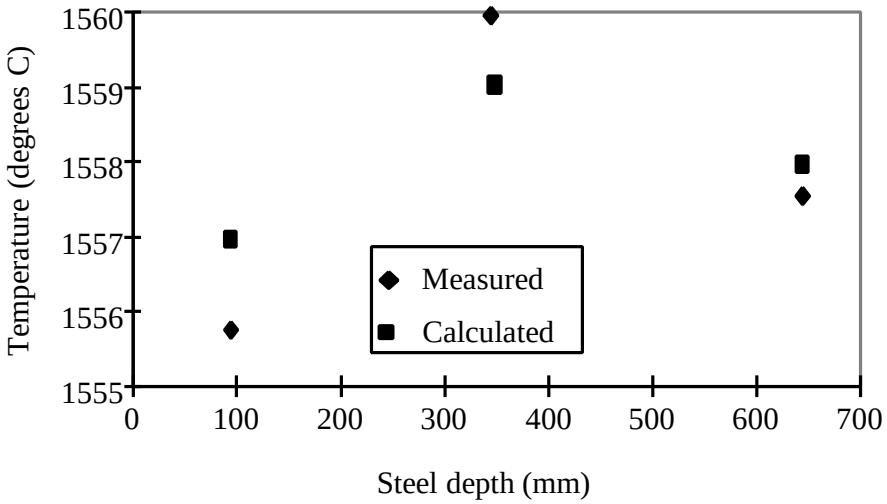

Fig. 4.5 - Predicted and measured steel temperatures as a function of steel depth.

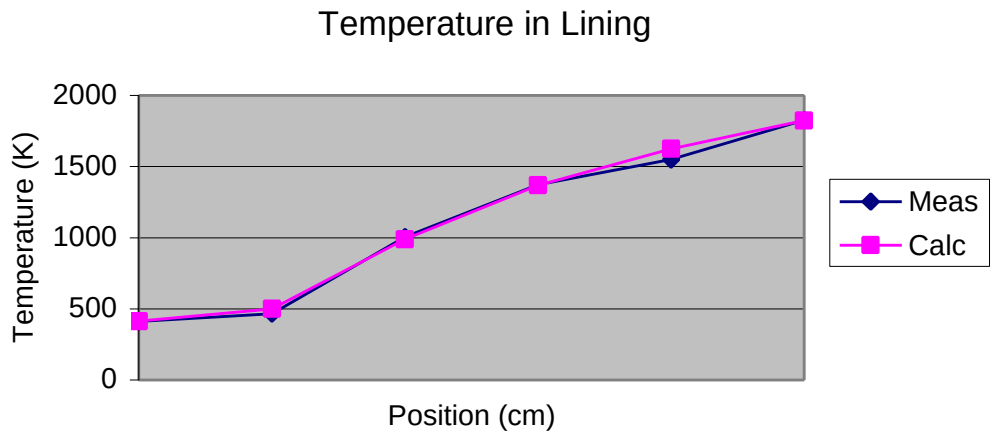

Fig. 4.6 - Measured and calculated temperatures in the refractory as function of position in the lining.

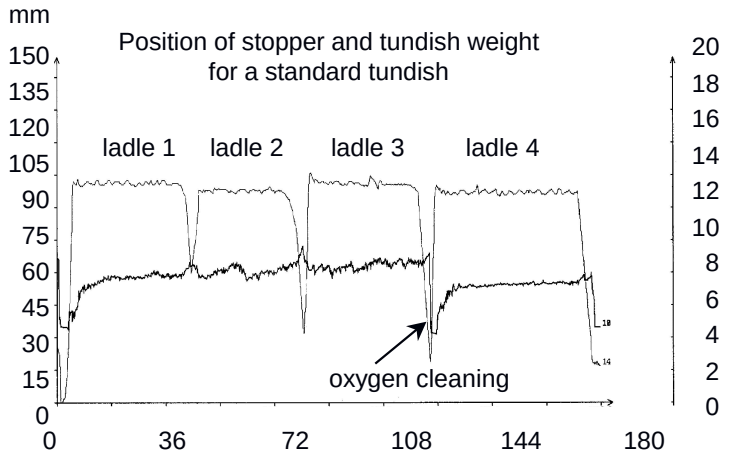

Fig. 4.7(a) - Heat changes and stopper rod movement during casting i a normal praxis tundish.

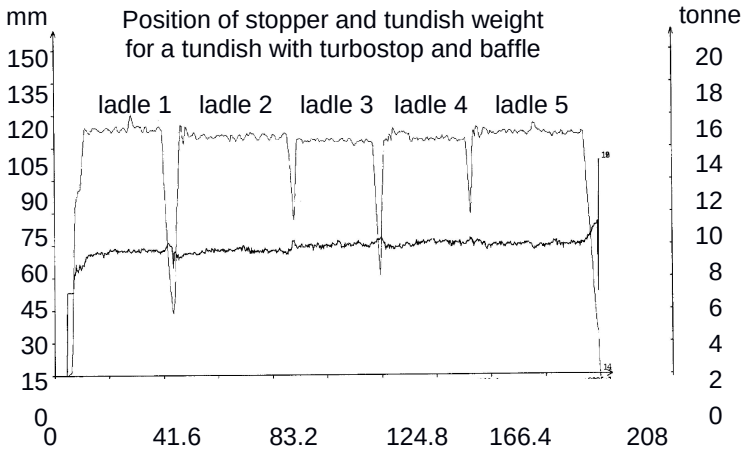

Fig. 4.7(b) - Heat changes and stopper rod movement during casting in a modified tundish.

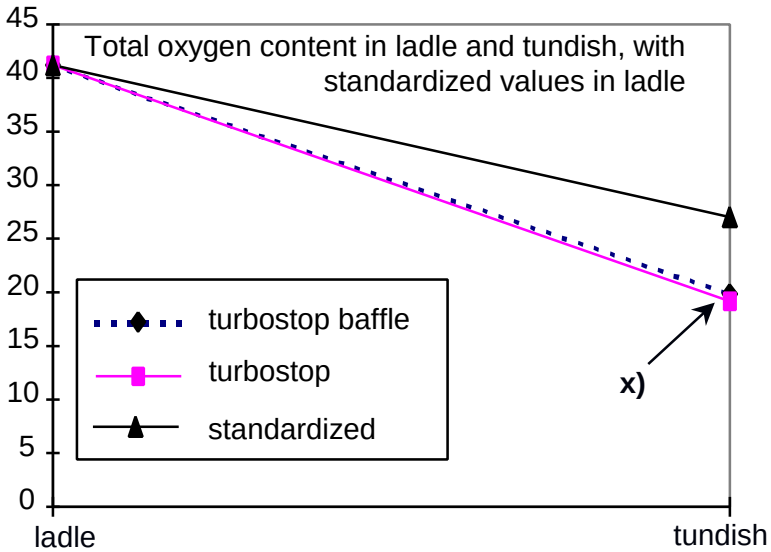

Fig. 4.7(c) - Steel cleanness in the tundish relative to steel cleanness in the ladle for both standard and modified tundish.

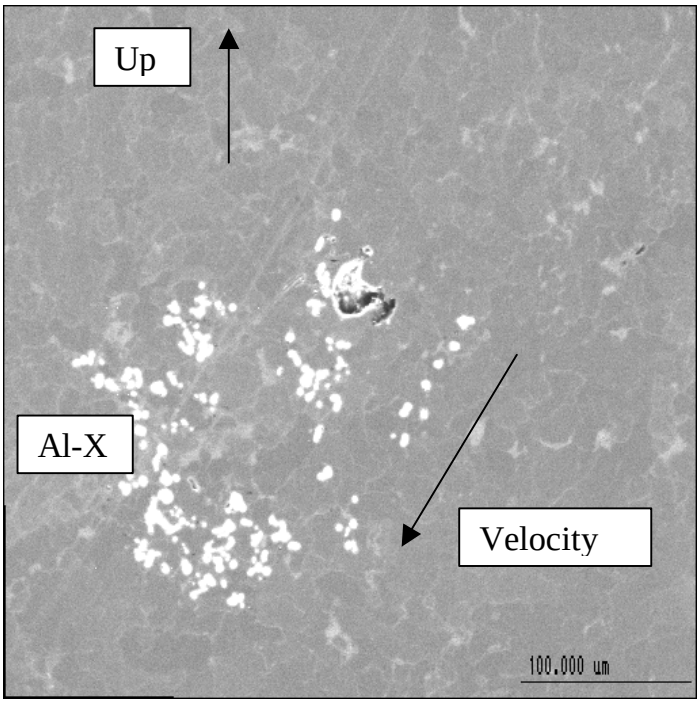

Fig. 4.8 - Rapidly rising, ~ 30 μm-large, “unstable” slag in low-carbon steel surrounded by small (< 2 μm) CaAl-AlO slag particles following the flow field approximately 8 mm below the steel/slag interface

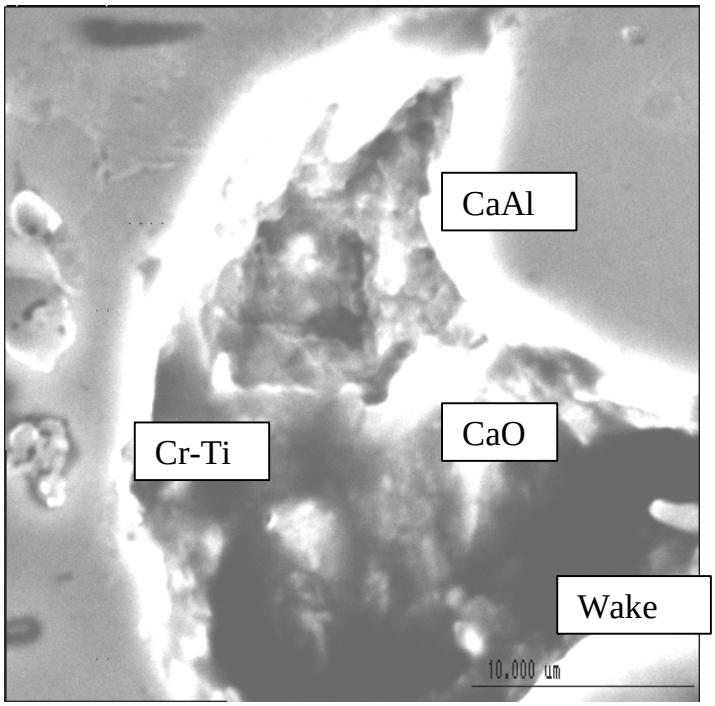

Fig. 4.9 - Detailed structure of the rising particle being an endothermic slag built on an exothermic Cr-Ti nucleus.

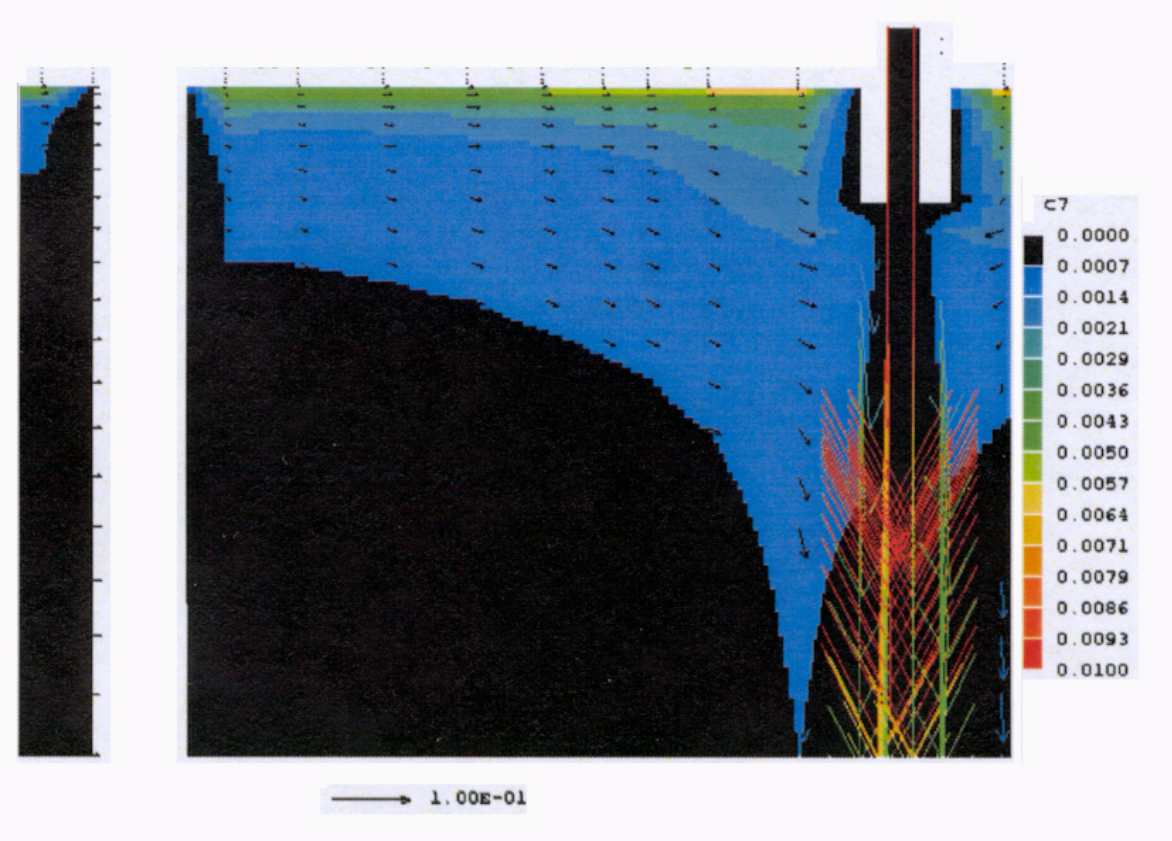

Fig. 5.1 - Velocity vectors superimposed on slag concentration profiles in the steel domain. Higher concentrations are found just below the steel/slag interface and where velocities have downwardly directed components.

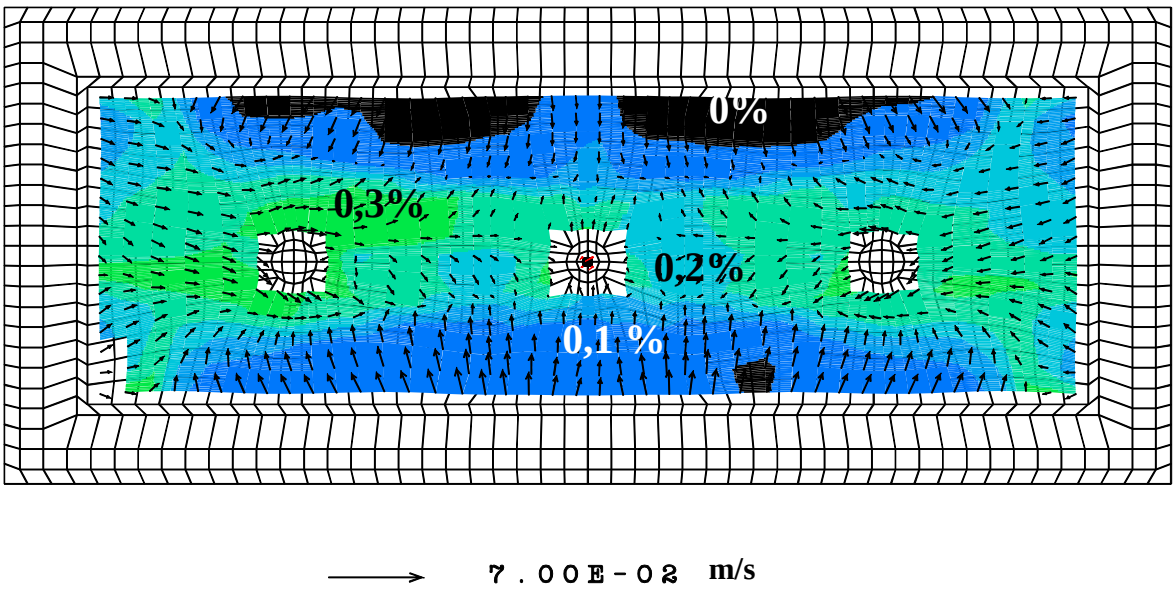

Fig. 5.2 - Slag concentrations in the upermost steel layer (3mm thick). In regions where the flow is upwards (black) the concentration is very low, indicating that steel is being pushed upwards.

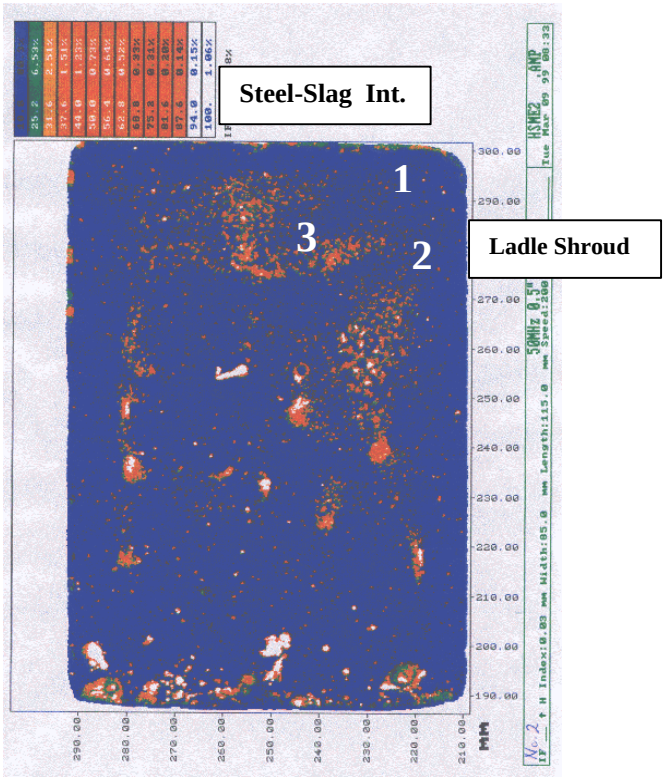

Fig. 5.3 - Image showing the distribution of rising slag particles and entrained slag particles along with the inevitable pores resulting from ultrasonic testing. The X-ray analysis positions are marked.

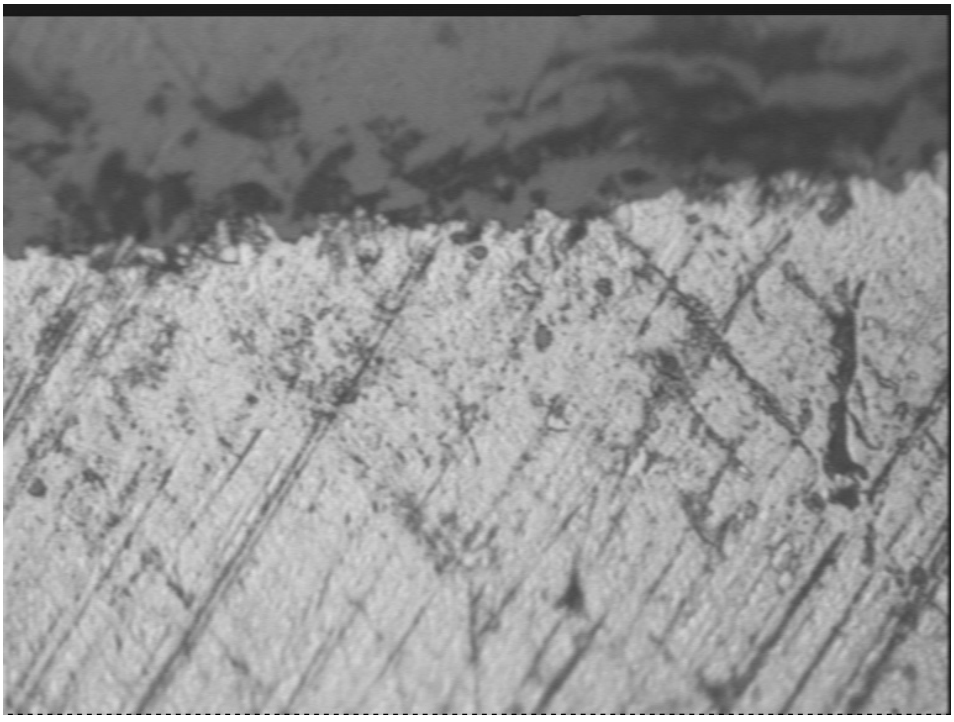

Fig. 5.4 - Instantaneously solidified steel-slag interface showing instabilities in the mixing zone.

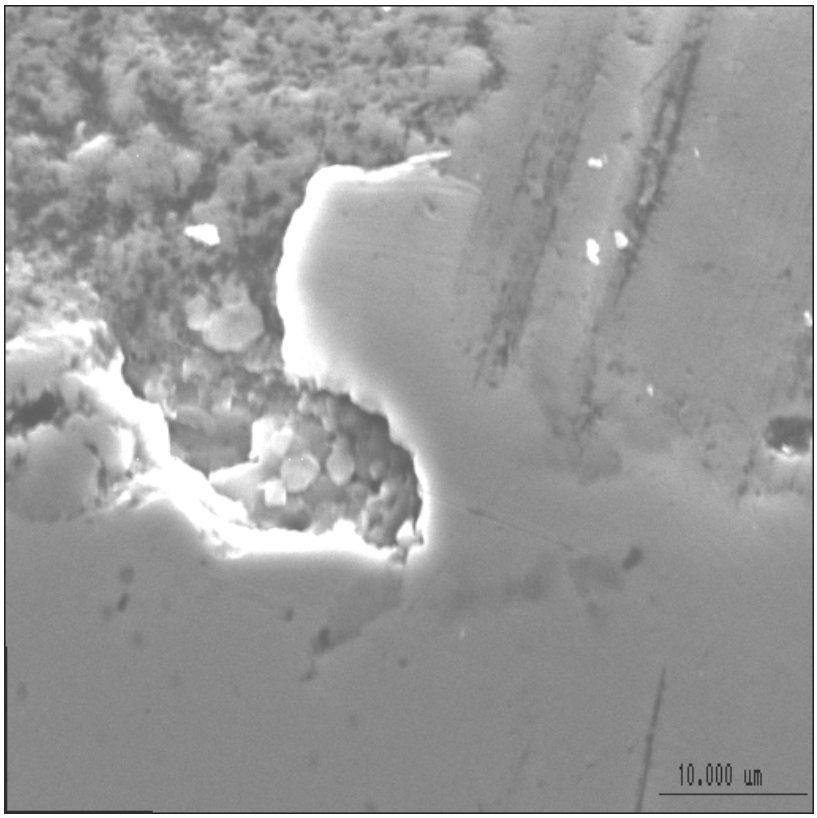

Fig. 5.5 - SEM-picture showing a probable Helmholz instability in the mixing zone containing oxides and salts.

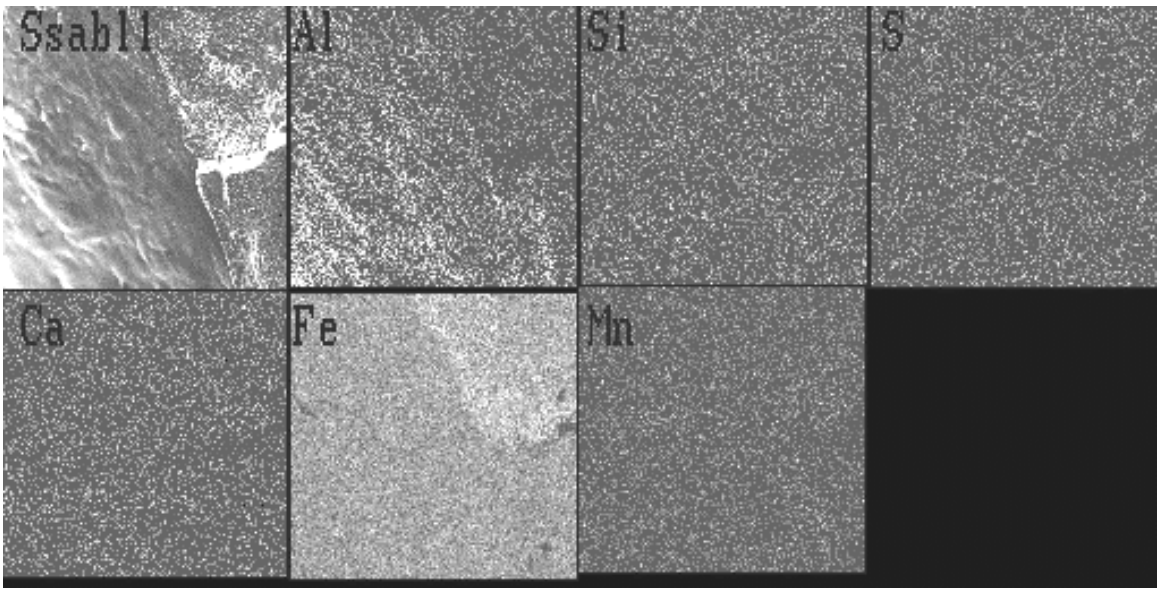

Fig. 5.6 - X-ray mapp of mixing zone showing component contents in different slag layers, also indicating Fe-content above the Al-layer.

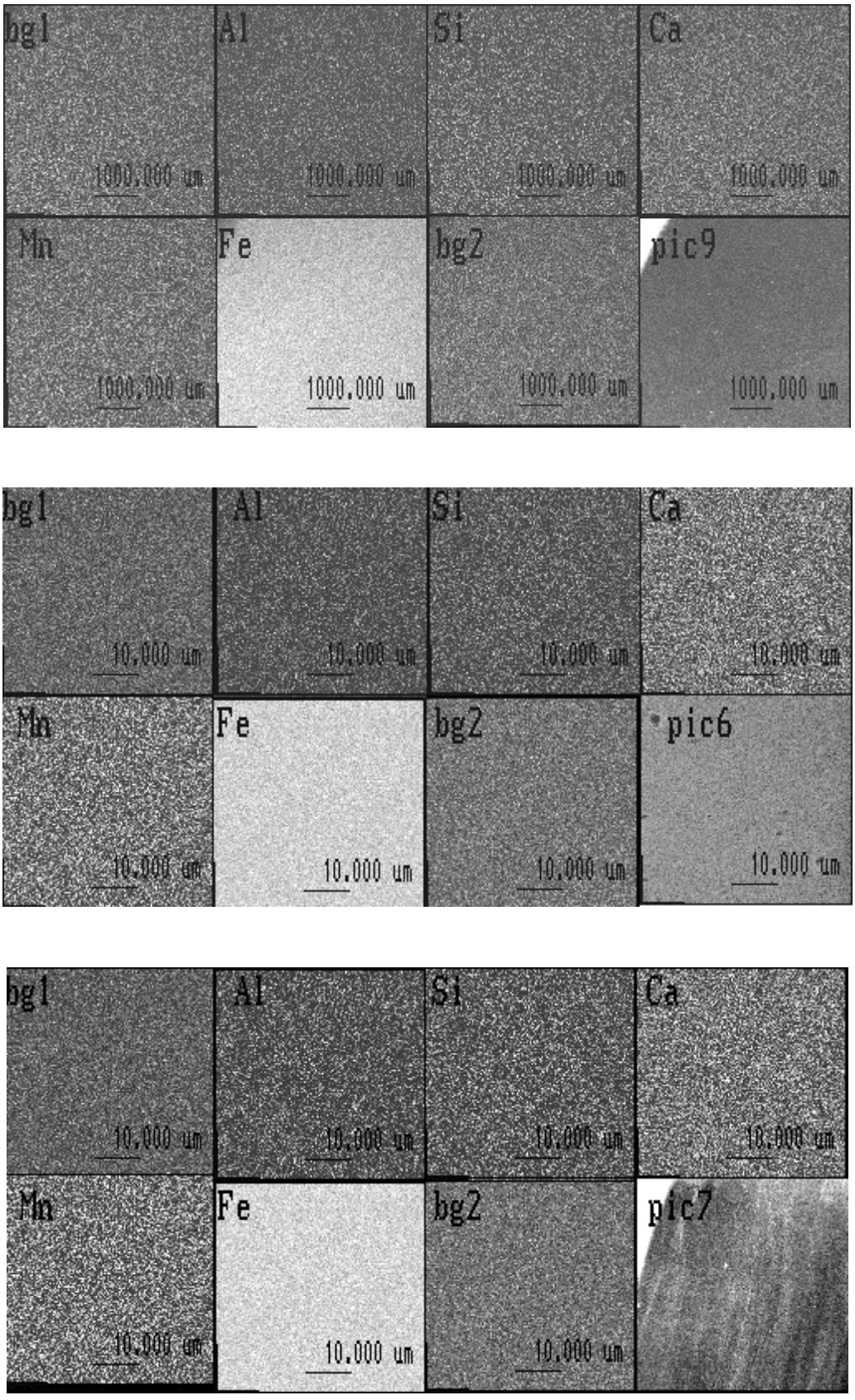

Fig. 5.7 - X-ray mapp at the tree positions in Figure 5.3 showing an encreasing Al-Si content towards point 3.

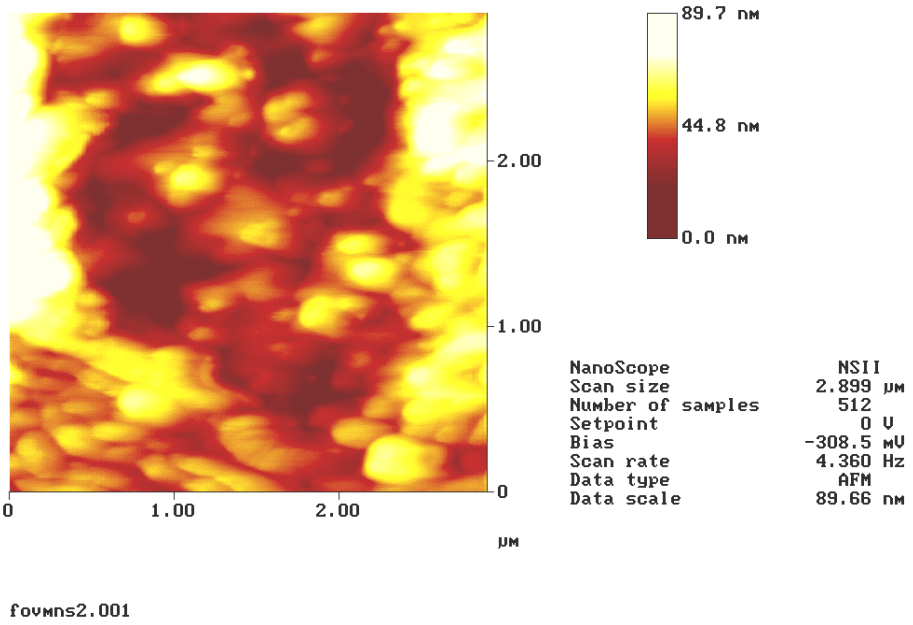

Fig. 5.8 - AFM-picture of MnS in perlite structure (bcc and fcc) showing well-developed bonds to the surounding matrix.

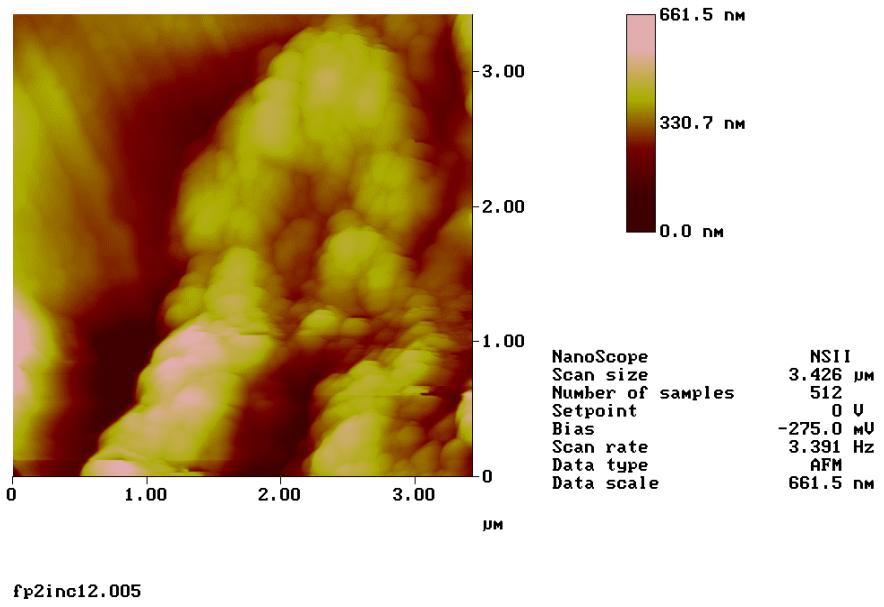

Fig. 5.9 - AFM-picture of Al-oxide illustrating developed voids in a surrounding ferrite (bcc) matrix.